Quantum-enhanced Doppler lidar

Citation for the original published paper (version of record):
Reichert, M., di Candia, R., Win, M. et al (2022). Quantum-enhanced Doppler lidar. npj Quantum Information, 8(1). http://dx.doi.org/10.1038/s41534-022-00662-9

ARTICLE OPEN

Check for updates

Quantum-enhanced Doppler lidar

Maximilian Reichert[1,2]✉, Roberto Di Candia[3,4], Moe Z. Win[5] and Mikel Sanz[1,2,6,7]✉

We propose a quantum-enhanced lidar system to estimate a target's radial velocity, which employs squeezed and frequency-entangled signal and idler beams. We compare its performance against a classical protocol using a coherent state with the same pulse duration and energy, showing that quantum resources provide a precision enhancement in the estimation of the velocity of the object. We identify three distinct parameter regimes characterized by the amount of squeezing and frequency entanglement. In two of them, a quantum advantage exceeding the standard quantum limit is achieved assuming no photon losses. Additionally, we show that an optimal measurement to attain these results in the lossless case is frequency-resolved photon counting. Finally, we consider the effect of photon losses for the high-squeezing regime, which leads to a constant factor quantum advantage higher than 3 dB in the variance of the estimator, given a roundtrip lidar-to-target-to-lidar transmissivity larger than 50%.

npj Quantum Information (2022)8:147 ; https://doi.org/10.1038/s41534-022-00662-9

INTRODUCTION

Quantum metrology exploits quantum mechanical resources, such as entanglement and squeezing, to measure a physical parameter with higher resolution than any strategy with classical resources. Many quantum metrology protocols in the photonic regime[1] have been proposed such as quantum illumination (QI)[2–6], quantum-enhanced position and velocity estimation[7–13], quantum phase estimation[14,15], transmission parameter estimation[16–20], noise estimation[21] and estimation of separation between objects[22,23], among others. In these protocols, information about an object is retrieved by interrogating it with a signal beam. In the most general strategy, this signal is correlated or entangled with an idler beam, which is retained in the lab to perform a joint measurement at the end of the protocol. Indeed, the scheme can be seen as an interferometer setup, in which a channel depending on the parameter of interest is only applied to the signal mode.

Of particular interest for remote sensing applications is the QI protocol, where the aim is to detect the presence of a weakly reflecting target with an error probability smaller than using the best classical strategy. Here, a quantum advantage in the error probability exponent can be achieved by using a global measurement (up to 6 dB)[24–28], or by using local measurements (up to 3 dB)[29–31]. This advantage is only achieved in a very noisy environment, such as the case of room-temperature microwave band, by a large bandwidth two-mode squeezed-vacuum state[3]. This requires a signal with a very low photon number per mode, which in the microwave regime is challenging to transmit open-air. Since amplifying the signal has been shown to break the quantum advantage[32,33], QI as originally thought remains an elusive achievement so far, even though recent progress has been made on relaxing the requirements for quantum advantage[34].

Once the presence of a target is established, properties like its location and velocity are also of interest. These can be estimated via signal arrival time and frequency measurement making use of the Doppler effect. Giovannetti, Lloyd and Maccone showed in ref. [7], that the GLM states, named after them, defined in the frequency domain can attain the Heisenberg limit (HL), which is a $1/N$ scaling of the estimation error of the arrival time, where N is the total number of photons. Equivalently, GLM states defined in the time domain reach the HL for the estimation error of frequency. This constitutes a quadratic improvement compared with the standard quantum limit (SQL) achieved by the classical protocol. In ref. [12], the simultaneous estimation of location and radial velocity was considered using two GLM states in the frequency and time domain, respectively, that are transformed into two entangled signal and idler beams via a beam splitter. It was shown that the velocity and the location can simultaneously be estimated achieving the Heisenberg limit. This proves that frequency entanglement lifts the Arthurs-Kelly relation[35], which states that the location and velocity of an object cannot be estimated with arbitrary precision using unentangled light. The work[13] further extended this by addressing the simultaneous estimation of relative location and velocity of two targets by means of two-photon entangled states. The main drawbacks of these previous works are the use of two-photon states, which does not allow for a photon-number-dependent analysis, and the use of the multiphoton GLM states, which are non-normalizable and thus not physical. In ref. [36], a normalized version of the GLM state was introduced for range estimation. Here, it was shown that the Heisenberg scaling persists for the normalized version. However, these GLM-type states are fragile in lossy channels. The loss of a single photon renders the state useless for retrieving information about the parameter. Although the robustness against losses of these GLM-type states may be improved by reducing their entanglement, this comes at the cost of decreasing the enhancement in the scaling of the error estimation. Furthermore, it is challenging to produce GLM states in the laboratory for photon numbers $N > 2$[9].

In this article, we propose a protocol for a quantum Doppler lidar, which estimates the radial velocity of a reflecting object using quantum light. As a probe state, frequency-entangled twin-beams are used. The signal beam is sent against the moving object, which causes a frequency shift due to the Doppler effect. Finally, a measurement of the returned signal and the idler is

[1]Department of Physical Chemistry, University of the Basque Country UPV/EHU, Apartado 644, 48080 Bilbao, Spain. [2]EHU Quantum Center, University of the Basque Country UPV/EHU, Bilbao, Spain. [3]Department of Information and Communications Engineering, Aalto University, Espoo 02150, Finland. [4]Department of Microtechnology and Nanoscience (MC2), Chalmers University of Technology, SE-41296 Göteborg, Sweden. [5]Laboratory for Information and Decision Systems, Massachusetts Institute of Technology, Cambridge, MA 02139, USA. [6]Basque Center for Applied Mathematics (BCAM), Alameda de Mazarredo 14, 48009 Bilbao, Spain. [7]IKERBASQUE, Basque Foundation for Science, Plaza Euskadi 5, 48009 Bilbao, Spain. ✉email: maximilian.reichert@ehu.eus; mikel.sanz@ehu.eus

performed. We propose for the protocol a multimode probe state that can be generated by a parametric downconverter. The state is composed of photon pairs that share frequency entanglement. This photon-pair structure is resilient against losses, since the loss of a single photon only effects its partner, but not the other photon pairs. This is a crucial difference with GLM states, where the loss of a single photon means the loss of all the information about the parameter of interest due to the global entanglement. The quantum protocol is benchmarked against a classical protocol shining the object with the same energy and for the same time duration to make the comparison fair. We employ the Quantum Fisher information (QFI) as the figure of merit in the comparison, since it gives the maximal amount of extractable information about the parameter of interest. Calculating the QFI for this multimode state is challenging, but by using properties of Gaussian states and introducing Schmidt modes, which effectively discretizes the frequency-continuous problem, we derive an analytical expression for the QFI. Two quantum resources can be identified in our resource quantum state, namely, squeezing and frequency entanglement. The performance of the quantum protocol is studied as a function of the photon number in three different parameter regimes, called high-frequency entanglement, high-squeezing, and mixed regime. The latter, for which a remarkable Heisenberg scaling can be attained, is called in this manner because neither squeezing nor frequency entanglement are dominant. We propose a measurement setup that attains the QFI, consequently achieving the highest estimation accuracy of the velocity. It is noteworthy that the measurement setup can be performed separately in the signal and the idler, facilitating the experimental requirements.

The paper is structured as follows. In Sections "Quantum estimation theory" and "Gaussian states", the fundamentals of quantum estimation theory and Gaussian states are introduced. In Section "Model of the moving target", we model the moving target as a perfectly reflective mirror boosted at a relative constant velocity. Afterwards in sections "Classical protocol and Quantum protocol", we introduce the probe states employed in both the quantum and classical protocols. As a figure of merit to benchmark their performance, we make use of the QFI. Then, in Section "A fair comparison", we discuss the different parameter regimes obtained and study when quantum advantage exists and how it behaves as a function of the signal photon number. In section A loss analysis for the high-squeezing regime, the protocol is studied in the presence of losses in the signal beam. Finally, in section A loss analysis for the high-squeezing regime an optimal measurement attaining the ultimate precision set by the quantum Cramér-Rao bound is provided.

RESULTS

Model of the moving target

We model the object of which we wish to estimate its constant radial velocity v relative to emitter as a perfect mirror in a $(1+1)$-dimensional spacetime. For now, we assume an absence of noise and loss. As can be seen in Fig. 1, the quantum Doppler lidar emits a signal beam towards the moving object, while also emitting an idler beam which is retained in the laboratory, such that a measurement can be performed of the returned signal and the idler. The electromagnetic field of the signal beam obeys the wave equation $(\partial_t^2 - c^2\partial_x^2)\phi(t,x) = 0$, where c is the speed of light and we only consider one polarization of the field for the sake of simplicity. The presence of the target which is modelled as a perfect mirror imposes the boundary condition $\phi(t, x_m) = 0$, where $x_m = vt$ is the location of the mirror. We assume the emitter to be to the right of the mirror, which corresponds to its spatial coordinate $> x_m$. The general solution of the wave equation

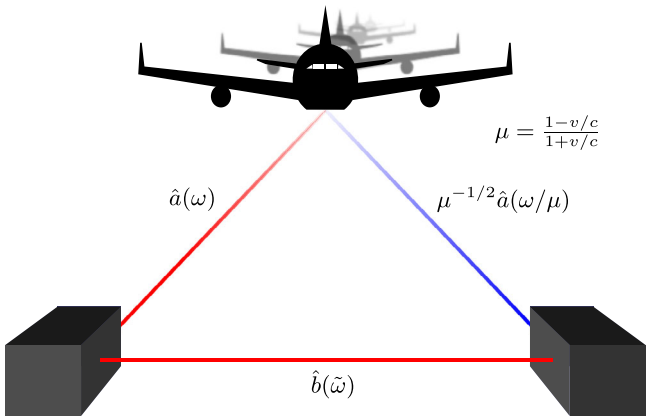

Fig. 1 Scheme of a quantum Doppler lidar. A twin-beam multimode squeezed-vacuum state is produced by the transmitter on the bottom left. The signal beam is sent towards the moving target where it is reflected and its frequency Doppler shifted. The idler beam does not interact with the moving target and is retained. Both the reflected signal beam and the idler beam are measured at the receiver on the bottom right.

satisfying the boundary condition is given by

$$\phi(x,t) = \int_0^\infty \frac{\mathrm{d}\omega}{\sqrt{4\pi\omega}} \left(\mathrm{e}^{-\mathrm{i}\omega(ct+x)} - \mathrm{e}^{-\mathrm{i}\frac{\omega}{\mu}(ct-x)}\right) a(\omega) + h.c. \tag{1}$$

where $\mu = (1 - v/c)/(1 + v/c)$ is the Doppler parameter. We choose to estimate the parameter μ instead of v, as it naturally arises in the Doppler effect. The estimation error of v is related to the one of μ via the error propagation formula for the QFI $J(v) = (\partial_v \mu(v))^2 J(\mu(v))$. The Fourier coefficients $a(\omega)$ and their complex conjugates get promoted by canonical quantization to annihilation and creation operators, which we denote by $\hat{a}(\omega)$ and $\hat{a}^\dagger(\omega)$. They satisfy the relations $[\hat{a}(\omega), \hat{a}(\tilde{\omega})] = [\hat{a}^\dagger(\omega), \hat{a}^\dagger(\tilde{\omega})] = 0$ and $[\hat{a}(\omega), \hat{a}^\dagger(\tilde{\omega})] = \delta(\omega - \tilde{\omega})$. The idler frequency mode is referred to as $b(\omega)$ and satisfies the same commutation relations. It commutes with the signal mode as both beams are spatially separated. The first term in Eq. (1) in brackets represents the incoming wave, while the second term is the outgoing wave which is Doppler shifted $\omega \to \omega/\mu$. Now, let us derive the Bogoliubov transformation $\hat{U}_\mu$ which maps the incoming modes $\hat{a}(\omega)$ to the Doppler reflected outgoing modes, denoted as $\hat{a}(-\omega)$. For this, a change of integration variables is performed in the second term in Eq. (1), leading to

$$\hat{\phi}(x,t) = \int_0^\infty \frac{\mathrm{d}\omega}{\sqrt{4\pi\omega}} \left(\mathrm{e}^{-\mathrm{i}\omega(ct+x)}\hat{a}(\omega) + \mathrm{e}^{-\mathrm{i}\omega(ct-x)}\hat{a}(-\omega) + h.c.\right),$$

with the operator $\hat{a}(-\omega) \equiv -\mu^{1/2}\hat{a}(\mu\omega)$. Thus, the process of reflection is described by the unitary transformation $\hat{U}_\mu \hat{a}(\omega)\hat{U}_\mu^\dagger = -\mu^{-1/2}\hat{a}(\omega/\mu)$. The prefactor $\mu^{-1/2}$ ensures a proper normalization and the change of sign is the π phase shift that radiation experiences when reflected. The vacuum state $|0\rangle$, which satisfies $\hat{a}(\omega)|0\rangle = \hat{b}(\omega)|0\rangle = 0$, remains unchanged after Doppler reflection, that is $U_\mu|0\rangle = |0\rangle$. In the most general framework, the outgoing mode also picks up a phase factor $\exp(\mathrm{i}2\omega x_m/(c-v))$ depending on the velocity and location x_m of the object. Therefore, this phase could in principle also be used to estimate the velocity, but generally at the cost of an additional knowledge about the location. Furthermore, in real world applications the phase often is randomized due to surface properties of the object and information about v is lost. Hence, as a first step, we will neglect the information from the phase and we will only consider the information about the velocity that is encoded in the frequency spectrum of the light beams. The QFI J_q derived here is a lower bound of the QFI in which phases are also taken into account.

Classical protocol

In the classical protocol we take a coherent signal as the probe state. For a continuum of frequency modes, a coherent state is defined as $|\psi\rangle = \exp[\alpha \int d\omega f(\omega)(\hat{a}(\omega) - \hat{a}^\dagger(\omega))]|0\rangle$, where we take the displacement constant α to be a real number for the sake of simplicity. The spectral amplitude $f(\omega)$ shall be an arbitrary differentiable and normalized function, i.e. $\int d\omega |f(\omega)|^2 = 1$. We assume that the carrier frequency $\omega_c = \int d\omega |f(\omega)|^2 \omega$ is much larger than the bandwidth $\Delta\omega$ defined as $\Delta\omega^2 = \int d\omega |f(\omega)|^2 (\omega - \omega_c)^2$, the so-called narrow-bandwidth approximation. This allows us to change the limits of integration to $(-\infty, \infty)$. The reflected state is given by $\hat{U}_\mu|\psi\rangle = |\psi_\mu\rangle = \exp[\alpha \int d\omega \mu^{1/2} f(\mu\omega)(\hat{a}^\dagger(\omega) - \hat{a}(\omega))]|0\rangle$, where we have used $\hat{U}_\mu e^{\hat{A}} \hat{U}_\mu^\dagger = e^{\hat{U}_\mu \hat{A} \hat{U}_\mu^\dagger} = e^{\hat{A}_\mu}$, and $\hat{A}$ is the exponent of the coherent state. Thus, the state is still a coherent state after the reflection but with an amplitude $f(\omega) \to -\mu^{1/2} f(\mu\omega)$. The mean frequency is shifted to ω_c/μ and the spectral bandwidth is stretched or compressed by a factor of $1/\mu$, see Supplementary Note 2. Therefore, estimating the frequency and the variance provides information about the parameter μ. The calculation of the QFI is straightforward, we need to compute $|\partial_\mu \psi_\mu\rangle$. As $[\partial_\mu \hat{A}_\mu, \hat{A}_\mu] = 0$, we can write $|\partial_\mu \psi_\mu\rangle = e^{\hat{A}_\mu} \partial_\mu \hat{A}_\mu |0\rangle$. As a consequence, it follows that $\langle \psi_\mu | \partial_\mu \psi_\mu \rangle = 0$ and $\langle \partial_\mu \psi_\mu | \partial_\mu \psi_\mu \rangle = \langle 0 | \partial_\mu \hat{A}_\mu^\dagger \partial_\mu \hat{A}_\mu | 0 \rangle$. This leads to the expression for the QFI (see Supplementary Note 2)

$$J_c(\mu) = \frac{4\alpha^2}{\mu^2} \int d\omega \left(\frac{1}{2} f(\omega) + \omega \partial_\omega f(\omega) \right)^2. \tag{2}$$

This is the general expression for the QFI. Let us now make some approximations to gain physical insights. First, we consider small velocities compared to the speed of light $v/c \ll 1$, for which the frequency Doppler shift is approximately $2\omega_c v/c$. Let us now introduce the spectral amplitudes' Fourier transform $g(t) = \int d\omega f(\omega) e^{i\omega t}$. The time duration ΔT of the pulse is given by $\Delta T^2 = \int dt\, t^2 |g(t)|^2 - \left(\int dt t |g(t)|^2 \right)^2$. Using the further approximation $\Delta T \Delta\omega v/c \ll 1$, which is standard in the classical literature[37], we obtain (for more details see Supplementary Note 2)

$$J_c(\mu) \approx \frac{4}{\mu^2} \omega_c^2 N_c \Delta T^2. \tag{3}$$

We see that the classical protocol follows the SQL scaling expected for a classical strategy. Furthermore, we note that three parameters completely define the optimal performance of a classical lidar, the photon number $\alpha^2 = N_c$, the carrier frequency ω_c and the time duration ΔT of the pulse.

Quantum protocol

For the quantum protocol, we use a twin-beam multimode squeezed-vacuum state. This state can be produced in the laboratory by non-linear optical processes, such as spontaneous parametric down-conversion (SPDC). In this process of SPDC, a pump beam, which is considered to be classical, interacts with a $\chi^{(2)}$ non-linear optical medium. Photons of the pump field decay into signal and idler photon pairs. The use of a waveguide for SPDC allows for reducing the number of spatial modes to one for each beam[38–42] given by $\hat{a}(\omega)$ (signal) and $\hat{b}(\tilde{\omega})$ (idler). The effective Hamiltonian describing the process is given by[43]

$$\hat{H}_I = i\hbar\xi \int d\omega \int d\tilde{\omega} f(\omega, \tilde{\omega}) \hat{a}(\omega) \hat{b}(\tilde{\omega}) + h.c., \tag{4}$$

where the coupling constant ξ, referred to as the squeezing parameter, is chosen to be real for simplicity, and proportional to the intensity of the classical pump beam and the strength of the interaction. The normalized joint-spectral amplitude $f(\omega, \tilde{\omega})$ depends on the specifics of the non-linear process and on the pump beam. In the case of SPDC, the joint-spectral amplitude can be in many cases approximated as a double Gaussian[44] which also simplifies analytic calculations

$$f(\omega, \tilde{\omega}) = \sqrt{\frac{2}{\pi\sigma\epsilon}} \exp\left(-\frac{(\omega + \tilde{\omega} - \omega_0)^2}{2\sigma^2} \right) \times \exp\left(-\frac{(\omega - \tilde{\omega})^2}{2\epsilon^2} \right). \tag{5}$$

The first exponential function in Eq. (5) with argument $\omega + \tilde{\omega}$ comprises energy conservation of the photon decay process and it is inherited by the frequency mode spectrum of the pump beam, which is assumed to be Gaussian with mean frequency ω_0 and variance $\sigma^2/2$. The second exponential function with argument $\omega - \tilde{\omega}$ corresponds to the phase matching condition, i.e. momentum conservation of the photon decay process, and depends on the spatial properties of the pump beam and the non-linear medium. Thus, by modifying the pump beam, both functions composing $f(\omega, \tilde{\omega})$ can independently be tailored[42]. We again assume the narrow-bandwidth approximation $\omega_0 \gg \sigma$ and $\omega_0 \gg \epsilon$. The double Gaussian can be decomposed into its Schmidt modes[45] as $f(\omega, \tilde{\omega}) = \sum_{n=0}^{\infty} r_n \psi_n(\omega - \omega_0/2) \psi_n(\tilde{\omega} - \omega_0/2)$, where $\{\psi_n(\omega)\}$ is an orthonormal set closely related to the Hermite functions (further details in Supplementary Note 3). The relative weight r_n^2 of each individual mode is given by $r_n = \frac{2\sqrt{\sigma\epsilon}}{\sigma+\epsilon} \left(\frac{\sigma-\epsilon}{\sigma+\epsilon} \right)^n$ with $\sum r_n^2 = 1$. The number of active modes is given by the Schmidt number $K = (\sum_n r_n^4)^{-1} = \frac{\sigma^2+\epsilon^2}{2\sigma\epsilon}$, which we interpret as a measure of frequency entanglement within the signal and idler photon pair. For $K = 1$, only one pair of modes is necessary to describe the state and the double Gaussian factorizes, that is $f(\omega, \tilde{\omega}) = \psi_0(\omega - \omega_0/2)\psi_0(\tilde{\omega} - \omega_0/2)$, which implies no frequency entanglement. For $K > 1$, the state is frequency entangled and the degree of entanglement grows monotonically with K. In refs. [42,46], techniques were proposed to generate Schmidt numbers in the range of $K \sim 400$–5000, which corresponds to an extremely high-frequency entanglement of the photon pair. The Schmidt modes capture the spectral structure of $f(\omega, \tilde{\omega})$ in a discrete manner, and thus it is natural to introduce discrete annihilation and creation operators $\hat{a}_n = \int d\omega \psi_n(\omega - \omega_0/2)\hat{a}(\omega)$ and $\hat{b}_n = \int d\omega \psi_n(\omega - \omega_0/2)\hat{b}(\omega)$ which are smeared out versions of $\hat{a}(\omega)$ and $\hat{b}(\tilde{\omega})$[47]. The modes satisfy the commutation relations $[\hat{a}_n, \hat{a}_m] = [\hat{b}_n, \hat{b}_m] = [\hat{a}_n, \hat{b}_m^\dagger] = 0$ and $[\hat{a}_n, \hat{a}_m^\dagger] = [\hat{b}_n, \hat{b}_m^\dagger] = \delta_{nm}$ due to the orthonormality of $\{\psi_n(\omega)\}$. The discrete description of the problem substantially facilitates the calculation of the QFI. The Hamiltonian in Eq. (4) is given in the discrete description by

$$\hat{H}_I = i\hbar\xi \sum_{n=0}^{\infty} r_n \left(\hat{a}_n \hat{b}_n - \hat{a}_n^\dagger \hat{b}_n^\dagger \right) \equiv i\hbar\xi \sum_{n=0}^{\infty} \hat{H}_n. \tag{6}$$

As the Hamiltonians for the individual modes commute $[\hat{H}_n, \hat{H}_m] = 0$, the total squeezing operator $\hat{S} = e^{-i\hat{H}_I/\hbar}$ of the SPDC process can be written as a tensor product of squeezing operators for each individual mode $\hat{S} = \bigotimes_{n=0}^{\infty} \hat{S}_n$ with $\hat{S}_n = e^{\xi \hat{H}_n}$. The squeezing parameter of the squeezer corresponding to the mode n is given by ξr_n. Finally, we are able to express the probe state of the quantum protocol using discrete creation operators. Using the normal ordered representation of squeezing operators[48], we find (see Supplementary Note 4 for details)

$$\hat{S}|0\rangle = \bigotimes_{n=0}^{\infty} \frac{1}{\cosh(\xi r_n)} \exp\left(-\tanh(\xi r_n) \hat{a}_n^\dagger \hat{b}_n^\dagger \right) |0\rangle. \tag{7}$$

Thus, the twin-beam multimode squeezed-vacuum state is just the product state of independent two-mode squeezed-vacuum states. Now, the reflected state $|\psi_\mu\rangle = \hat{U}_\mu \hat{S}|0\rangle$ is

$$|\psi_\mu\rangle = \mathcal{N} \exp\left(-\sum_{n=0}^{\infty} \tanh(\xi r_n) \hat{a}_{n\mu}^\dagger \hat{b}_n^\dagger \right) |0\rangle, \tag{8}$$

where we have transformed the product in Eq. (7) into a sum in the exponent and we have introduced the normalization constant $\mathcal{N} = \prod_n 1/\cosh(\xi r_n)$, which is independent of μ. The operator $\hat{a}_n^\dagger$ transforms into $\hat{U}_\mu \hat{a}_n \hat{U}_\mu^\dagger = \hat{a}_{n\mu}^\dagger = -\int \mathrm{d}\omega \mu^{1/2} \psi_n(\mu\omega - \omega_0/2)\hat{a}^\dagger(\omega)$, picking up a phase shift and a μ-dependence, whereas ξ, r_n, and the idler modes $\hat{b}_n$ remain μ-independent. The mean frequency of the transformed mode is given by $\omega_0/2\mu = \overline{\omega}$, as one would expect from the Doppler effect. The bandwidth of each mode is proportional to $\sqrt{\sigma\epsilon/2}$, and it transforms into $\sqrt{\sigma\epsilon/2\mu} \equiv \overline{\sigma}$ after the reflection. In the continuous formalism, the joint-spectral amplitude converts into $f(\omega, \tilde{\omega}) \to -\mu^{1/2} f(\mu\omega, \tilde{\omega})$. Now, in order to calculate the QFI, we need to first evaluate the derivative $|\partial_\mu \psi_\mu\rangle$. The only component of the state that depends on μ is $\hat{a}_{n\mu}^\dagger$. The derivative can be calculated using the properties of the Hermite functions and we find that $\partial_\mu \hat{a}_{n\mu}^\dagger$ is a linear combination of creation operators $\hat{a}_{n\mu}^\dagger$ ranging from modes $n-2$ to $n+2$. As the derivative of the exponent in Eq. (8) commutes with the exponent itself, we find $|\partial_\mu \psi_\mu\rangle = -\sum_n \tanh(\xi r_n)(\partial_\mu \hat{a}_n^\dagger)\hat{b}_n^\dagger S|0\rangle$, see Supplementary Note 5. By using the transformation rule $\hat{S}^\dagger \hat{a}_{n\mu} \hat{S} = \hat{a}_{n\mu}\cosh(\xi r_n) - \hat{b}_n^\dagger \sinh(\xi r_n)$ and the analogous rule for the idler mode, whose derivation is discussed in Supplementary Note 4, we finally find the analytic expression for the QFI (see Supplementary Note 5 for the full derivation). This splits up into frequency and mode-bandwidth contributions as $J_q(\mu) = (\partial_\mu \overline{\omega})^2 J_q(\overline{\omega}) + (\partial_\mu \overline{\sigma})^2 J_q(\overline{\sigma})$ with

$$J_q(\mu) = \frac{1}{\mu^2}\frac{\omega_0^2}{\sigma\epsilon}\left(Z_{\overline{\omega}} + \frac{\sigma\epsilon}{\omega_0^2} Z_{\overline{\sigma}}\right), \tag{9}$$

with the frequency term defined as

$$Z_{\overline{\omega}} = \sum_{n=0}^{\infty} \sinh^2(\xi r_n)\left(n\cosh^2(\xi r_{n-1}) + (n+1)\cosh^2(\xi r_{n+1})\right) \tag{10}$$

and the mode-bandwidth term as

$$\begin{aligned} Z_{\overline{\sigma}} = \sum_{n=0}^{\infty} \sinh^2(\xi r_n)\big(&n(n-1)\cosh^2(\xi r_{n-2}) \\ &+ (n+1)(n+2)\cosh^2(\xi r_{n+2})\big). \end{aligned} \tag{11}$$

The bandwidth contribution is suppressed by the factor $\sigma\epsilon/\omega_0^2$ as can be seen in Eq. (9), which is small due to the narrow-bandwidth approximation. For a typical SPDC process in potassium dihydrogen phosphate crystal pumped by a frequency doubled titanium-sapphire laser, this factor is approximately $\sqrt{\sigma\epsilon/\omega_0^2} \sim 0.01$[49].

A fair comparison

Let us now compare the performance of the quantum and the classical protocols and find out under which conditions quantum advantage is achieved. For that, we examine the quantum advantage ratio J_q/J_c, where we have omitted the dependence on μ for the sake of readability. In the case $J_q/J_c > 1$, the quantum strategy outperforms the classical one assuming that an optimal measurement is performed and the Cramér-Rao bound is attained, which is usually the case in the absence of thermal noise photons. We already pointed out in Section "Classical protocol", that the classical lidar is solely characterized by the three parameters photon number, carrier frequency and time duration. So to fairly compare both protocols, we set these three parameters equal for both signal beams. For photon number and mean frequency, this corresponds to $\omega_c = \omega_0/2$ and $a^2 = \sum_n \sinh^2(\xi r_n)$. Now, let us calculate the time duration of the quantum signal beam. For that we introduce the time-domain version of the creation and annihilation operators via $\hat{E}^\dagger(t) = \int \mathrm{d}\omega\, \mathrm{e}^{\mathrm{i}\omega t}\hat{a}^\dagger(\omega)$, which is the operator creating a photon at time t at the transmitter. The normalized power of the signal beam is defined as $|s(t)|^2 = \langle\psi|\hat{E}^\dagger(t)\hat{E}(t)|\psi\rangle/N_S$. The time duration can then be calculated and we find

$$\Delta T^2 = \int \mathrm{d}t\, t^2 |s(t)|^2 - \left(\int \mathrm{d}t t |s(t)|^2\right)^2 \tag{12}$$

$$= \frac{2}{\sigma\epsilon}\left(\frac{\sum_{n=0}^{\infty}\sinh^2(\xi r_n) n}{\sum_{m=0}^{\infty}\sinh^2(\xi r_m)} + \frac{1}{2}\right). \tag{13}$$

The detailed calculations can be found in Supplementary Note 5. As both J_q and ΔT are given by infinite series containing hyperbolic trigonometric functions, we will in the following study parameter regimes in which simple analytic expression for the respective quantities can be obtained, which helps to interpret the results.

No frequency entanglement

Let us first study the case in which no frequency entanglement is present between signal and idler beams. In this case, we have $K = 1$, i.e. $\sigma = \epsilon$. The state reduces to the well-known two-mode squeezed-vacuum state $|\psi_\mu\rangle = \exp(\xi(\hat{a}_{0\mu}\hat{b}_0 - \hat{a}_{0\mu}^\dagger \hat{b}_0^\dagger))|0\rangle$ with signal photon number $N_S = \sinh^2(\xi)$. We find that

$$\frac{J_q}{J_c} = 1 \tag{14}$$

for all values of the squeezing parameter ξ (Supplementary Note 6). Thus, no quantum advantage is achieved with a two-mode squeezed-vacuum state. Both protocols obey the SQL $J_q, J_c \sim N_S$. In similar interferometric phase estimation protocols, Heisenberg scaling is achieved with the two-mode squeezed state. But due to our ignorance of the target's position x_m, the information about the velocity contained in the phase $\exp(\mathrm{i}2\omega x_m/(c-v))$ cannot be accessed and thus Heisenberg scaling is not achievable in our case. Thus, frequency entanglement $K > 1$ is necessary for quantum advantage in our protocol with pure probe states given in Eq. (7).

High-frequency-entanglement regime

Let us now consider the case in which the frequency entanglement is the dominant quantum resource. We specify this regime by the condition $\xi \ll K^{1/2}$, which allows us to approximate the hyperbolic functions as $\sinh^2(\xi r_n) \approx \xi^2 r_n^2$ and $\cosh^2(\xi r_n) \approx 1$. The number of photons in mode n is given by $N_{Sn} = \sinh^2(\xi r_n) \ll 1$ and the total photon number can be approximated as $N_S \approx \xi^2$, where we have only taken the first term of the approximation into account (Supplementary Note 7). With this, the ratio of QFIs is

$$\frac{J_q}{J_c} \approx 1 + \frac{\sigma^2 + \epsilon^2}{2\omega_0^2}\left(1 + \frac{1}{K^2} + \frac{1}{K(K^2+K)}\right). \tag{15}$$

The first term is the frequency contribution and is equal to 1. The remaining terms correspond to the bandwidth contribution which is small due to the narrow-bandwidth approximation. Thus, in the high-frequency entanglement regime no quantum advantage can be obtained, the classical and quantum protocol perform equally well. With the further constraint $\xi \ll 1$, the state becomes a superposition of the vacuum and a two-photon state, the same state used in ref. [12,13]. Even though these states yield no quantum advantage in estimating the velocity alone, they yield advantage in jointly estimating the position and velocity of a target.

High-squeezing regime

Let us now consider a regime in which squeezing is the dominant quantum resource and the frequency entanglement is relatively

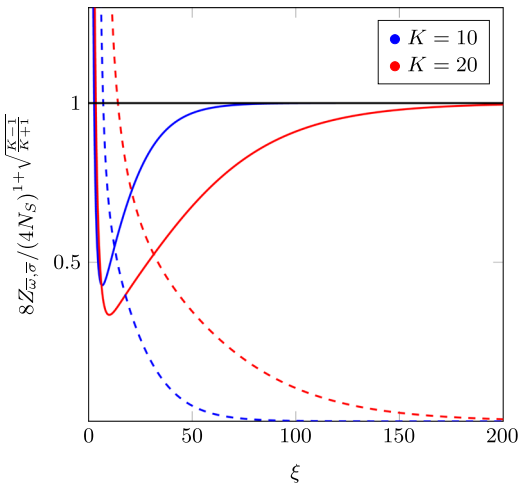

Fig. 2 The frequency and bandwidth contribution in the high-squeezing regime. The normalized frequency (solid lines) and bandwidth (dashed lines) contributions $8Z_{\overline{\omega},\overline{\sigma}}/(4N_S)^{\sqrt{\frac{K-1}{K+1}}}$ are plotted against the squeezing parameter ξ for Schmidt numbers $K = 10$ and $K = 20$. The normalized QFI approaches 1, which indicates a scaling above the SQL in the limit $K^{3/2} \ll \xi$. The normalized bandwidth contribution is much smaller and goes to 0 for $K^{3/2} \ll \xi$. It is even further suppressed by the factor $\sigma\epsilon/\omega_0^2$.

weak. We specify the parameter conditions as $\xi \gg K^{3/2}$ and $K \gtrsim 1.5$. These conditions helps us to put the QFI into a concise analytic form. Additionally, by requiring $K \gtrsim 1.5$, the high-squeezing regime is sufficiently distinct from the no-entanglement regime with $K = 1$. The details about the calculations performed in this Subsection can be found in Supplementary Note 8. The fraction of photons in the mode n is given by N_{Sn}/N_S, where $N_{Sn} = \sinh^2(\xi r_n)$ is the photon number of the mode n of the signal beam. By increasing ξ for a fixed K, the relative contribution of higher modes $n > 0$ decreases. In the high-squeezing regime, almost all the photons reside in the 0 mode, that is $N_S \approx N_{S0} \gg N_{S1} \gg 1$, implying a high photon number per mode but a low number of active modes, contrary to the high-frequency entanglement regime. With this, we arrive in the asymptotic limit at the result

$$\frac{J_q}{J_c} \approx \frac{1}{3}(4N_S)^{\sqrt{\frac{K-1}{K+1}}}, \tag{16}$$

where it was used that $N_{Sn} = \sinh^2(\xi r_n) \approx \cosh^2(\xi r_n)$ for $n = 0, 1$ and only terms of order $N_{S0}N_{S1}$ in Eq. (9) contribute significantly. This is the reason why the bandwidth terms are negligible. In Fig. 2, both the normalized frequency (solid lines) and bandwidth (dashed lines) terms are plotted against ξ for Schmidt numbers $K = 10$ and $K = 20$, confirming our analytical results. Interestingly, the QFI in terms of the mode photon numbers is $J_q \sim N_{S0}N_{S1}$, which indeed indicates a scaling better than the SQL, and nearly reaches the HL for K big enough. As a conclusion, increasing the squeezing for a fixed K also increases the quantum advantage, so squeezing can be seen as a sensitivity-enhancing resource of the protocol. Up to this point, photon loss and noise has been neglected. In section "A loss analysis" for the high-squeezing regime, the impact of losses, but not the impact of noise, will be examined on the high-squeezing regime.

The mixed regime

Now, let us study the intermediate parameter regime $K^{1/2} \ll \xi \ll K^{3/2}$. Under these conditions, multiple modes are active like in the high-frequency entanglement regime and the photon number per mode is high $N_{Sn} \gg 1$ like in the high-squeezing regime, hence the

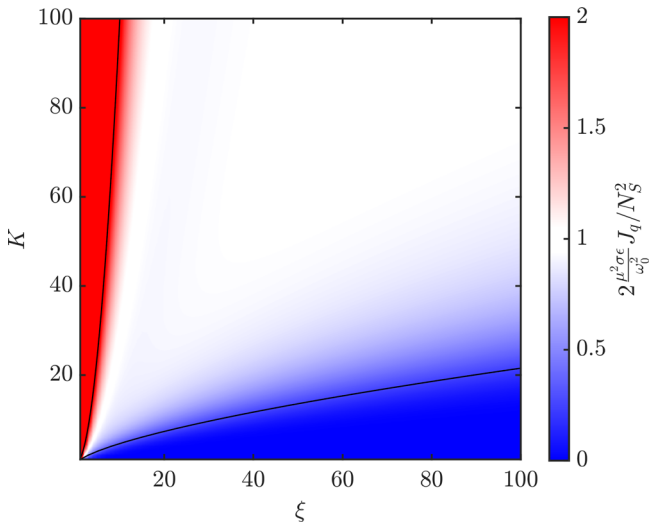

Fig. 3 The three parameter regimes. We plot the normalized QFI $2\frac{\mu^2\sigma\epsilon}{\omega_0^2}J_q/N_S^2$, not to be confused with the quantum advantage ratio. The plot shows the three parameter regimes and their corresponding borders given by the contours $\xi = K^{1/2}$ and $\xi = K^{3/2}$. The mixed regime is characterized by the value of 1, depicted as white, and thus shows Heisenberg scaling and validates our analytical expression for the QFI. The high-squeezing regime, in which quantum advantage above the SQL is achieved, is depicted as blue with values below 1. The red area is the high-entanglement regime, where the values range far above 2 but were cut off. In this regime, no quantum advantage is achieved.

name mixed regime. Using these conditions, we can derive in the asymptotic limit an analytic expression of the QFI

$$\frac{J_q}{J_c} \approx \left(\frac{\xi}{2^{1/2}K^{3/2}} + \frac{\sigma\epsilon}{4\omega_0^2}\right)N_S, \tag{17}$$

where the first term is again the frequency contribution and the second term the bandwidth contribution, following both a Heisenberg scaling $J_q \sim N_S^2$. For details about the calculations in this Subsection, see Supplementary Note 9. The factor $\xi/2^{1/2}K^{3/2}$ is smaller than 1, but we still have $(\xi/2^{1/2}K^{3/2})N_S \gg 1$ thus guaranteeing quantum advantage. Since both terms $\sigma\epsilon/4\omega_0^2$ and $\xi/2^{1/2}K^{3/2}$ are smaller than 1, we cannot generally decide which contribution is dominant. For instance, in the experimental setup referred to in section "Quantum protocol", we had that $\sqrt{\sigma\epsilon}/\omega_0 \sim 0.01$, the bandwidth can be safely neglected in the mixed regime, at least for values of ξ and K up to 100 as can be seen in Supplementary Note 9. Therefore, we will neglect the bandwidth contribution from this point on.

In Fig. 3, the ratio $\frac{2\mu^2\sigma\epsilon}{\omega_0^2}J_q/N_S^2 \approx 2Z_{\overline{\omega}}/N_S^2$ is plotted for both ξ and K up to the values of 100. Three distinct regions corresponding to the three parameter regimes can be appreciated. In the white area, which corresponds to a value of 1 for the ratio, we observe a behaviour of $J_q \sim N_S^2$ for the QFI and thus Heisenberg scaling. The red area is the high-frequency entanglement regime and the blue area is the high-squeezing regime. Curiously, quantum advantage is achieved in the two regimes with high photon number per mode, and not in the high-frequency entanglement regime with a low photon number per mode. This in contrast to the quantum illumination protocol, where a small photon number per mode is necessary to achieve quantum advantage. The parameter conditions of the three regimes and their corresponding quantum advantages are summerized in Table 1.

Table 1. Listed are the quantum advantages for the different parameter regimes.

Regime 1	Regime 2	Regime 3
$\xi \ll K^{1/2}$	$\xi \gg K^{3/2}$	$K^{1/2} \ll \xi \ll K^{3/2}$
$\frac{J_q}{J_c} \approx 1$	$\frac{J_q}{J_c} \sim N_S^{\frac{K-1}{K+1}}$	$\frac{J_q}{J_c} \sim \frac{\xi}{K^{3/2}} N_S$

Regime 1, 2 and 3 correspond to the high-frequency entanglement, the high-squeezing and the mixed regime, respectively. Here, the contributions due to the bandwidth shift are neglected.

A loss analysis for the high-squeezing regime

So far we have considered the ideal scenario in which no photons are lost and the returned state is pure. In realistic scenarios, the probe state at the receiver will be mixed due to photon loss and thermal noise. In ref. [11], time-of-flight estimation in the microwave regime was studied, in which the thermal photon number per mode is much larger than 1. A similar state was used, a continuous wave squeezed state, and a considerable quantum advantage was proved at a certain threshold of the signal-to-noise ratio. This so-called threshold effect arises only in the presence of thermal noise and requires an analysis that goes beyond the calculation of the QFI. In our protocol, we assume operation in the optical regime, in which thermal noise can be neglected and solely relying on the QFI suffices. Photon loss, however, has to be considered to assess if the protocol shows quantum advantage in more realistic scenarios. Because photon loss mixes the state, the calculation of the QFI is significantly more complicated. Thus, we will only study the high-squeezing regime in which the state can be described sufficiently well by only a couple of Schmidt modes and thus allows us to derive analytical expressions. We assume no losses in the idler beam. Photon loss in the signal beam can occur on the way to and from the target and/or during the interaction with the object (which generalizes the protocol to non-perfectly reflecting objects). The probability of losing a signal photon is assumed to be frequency-independent and it is modelled by a beam splitter

$$\hat{U}_B \hat{a}(\omega) \hat{U}_B^\dagger = \sqrt{\eta}\hat{a}(\omega) + \sqrt{1-\eta}\hat{c}(\omega), \tag{18}$$

where $\hat{c}(\omega)$ is an auxiliary mode which cannot be accessed by the experimenter and will be traced out at the end. In this framework, the beam splitter commutes with the Doppler reflection operation, so only one beam splitter with effective transmissivity η is required for the lidar-to-target-to-lidar roundtrip. We choose to apply this beam splitter operation after the reflection at the receiver level. The final state is a Gaussian state. Gaussian states are fully described by their first two moments $\mathbf{d}$ and Σ, the definitions and an introduction to Gaussian states can be found in section "Gaussian states" and ref. [50]. As we discussed in section "High-squeezing regime", only the first two pairs of modes $\hat{a}_{0\mu}, \hat{a}_{1\mu}$ and $\hat{b}_0, \hat{b}_1$ are populated with a significant amount of photons. This allows us to omit the rest of the modes by tracing them out and thus derive a lower bound for the QFI. Alternatively, we could justify the neglect of the higher modes by tailoring the joint-spectral amplitude $f(\omega, \tilde{\omega})$, such that only the first two modes are active. To use the formula for the QFI of Gaussian states given in ref. [50], we need to change the basis (i.e. the modes $\hat{a}_{0\mu}$ and $\hat{a}_{1\mu}$) to make it parameter independent. To do so, we assume that a prior estimate μ_0 of the parameter is known and we only want to estimate the small deviation δ with $\mu = \mu_0 + \delta$, which is standard in most parameter estimation protocols. We expand the Schmidt modes around μ_0 up to the first order and find

$$\hat{a}_{0\mu} \approx \hat{a}_{0\mu_0} - \delta \frac{\omega_0}{2\mu\sqrt{\sigma\epsilon}} \hat{a}_{1\mu_0} \tag{19}$$

$$\hat{a}_{1\mu} \approx \hat{a}_{1\mu_0} + \delta \frac{\omega_0}{2\mu\sqrt{\sigma\epsilon}} \left(\hat{a}_{0\mu_0} - \sqrt{2}\hat{a}_{2\mu_0} \right), \tag{20}$$

where we have neglected the terms corresponding to the bandwidth contribution, as they are small in this regime, which we have previously established in section "High-squeezing regime". Now, we have the modes $\hat{a}_{0\mu_0}, \hat{a}_{1\mu_0}, \hat{a}_{2\mu_0}, \hat{b}_0, \hat{b}_1, \hat{c}_{0\mu_0}, \hat{c}_{1\mu_0}, \hat{c}_{2\mu_0}$, where $\hat{c}_{n\mu_0} = \int d\omega \mu_0^{1/2} \psi_n(\mu_0\omega - \omega_0/2)\hat{c}(\omega)$ are the auxiliary Schmidt modes. The resulting covariance matrix and QFI are calculated in Supplementary Note 10. We recover the result from Eq. (16) for the lossless case $\eta = 1$, which confirms the validity of our approach and our approximations. To make a fair comparison, we also have to consider the classical protocol under the effect of photon loss. The QFI of the classical strategy is simply reduced by the factor η, that is $J_c \approx \eta\omega_0^2 N_S \Delta T^2/\mu^2$. We arrive at the ratio

$$\frac{J_q}{J_c} \approx \frac{1}{1-\eta}, \tag{21}$$

where we assumed $N_{S1}(1-\eta) \gg 1$ to obtain a compact result. This assumption causes the divergence in Eq. (21) since, as $\eta \to 1$, we have $N_{S1} \to \infty$. Without this assumption, we recover the result of the lossless scenario in the limit of $\eta \to 1$. The quantum advantage ratio in Eq. (21) does not depend on the photon number, and thus, photon loss destroys the near HL scaling and brings it down to the SQL, that is $J_q \sim N_S$. A constant factor quantum advantage is achieved for all values of η, but this factor becomes insignificant for small path transmissivities $\eta \ll 1$. For transmissivities $\eta \geq 50\%$, the quantum advantage factor is $J_q/J_c \geq 2 \approx 3$dB. This makes our protocol promising for short-range applications where the path losses are small, such as Doppler microscopy for biologicals.

Optimal measurement

As we are estimating only the velocity of the object, there always exists at least one optimal measurement saturating the QFI, but it is not necessarily unique. Quantum estimation theory provides techniques to construct some of these observables, in particular the one related to the symmetric logarithmic derivative (SLD) $\hat{O}_\mu = \mathbb{1}\mu + \hat{L}_\mu/J(\mu)$. However, its implementation in a realistic experimental setup is a highly non-trivial task. In the case of a pure-state manifold, the SLD $\hat{L}_\mu$ can be written as $\hat{L}_\mu = |\partial_\mu\psi_\mu\rangle\langle\psi_\mu| + |\psi_\mu\rangle\langle\partial_\mu\psi_\mu|$[51]. Thus, only $|\partial_\mu\psi_\mu\rangle$ needs to be calculated, which has been done for the calculation of the QFI and it can be found in Supplementary Note 5. However, a construction of this observable in a lab in an optical setup is far from trivial. Furthermore, it depends on the parameter μ itself, and we would like to have a measurement working on the whole range of velocities if possible. Otherwise, an adaptive measurement strategy could be followed[52]. In the Gaussian formalism, the SLD can be written as a sum of terms that are at most quadratic in the modes[50]. In Supplementary Note 10 we have given the explicit expression for the SLD derived in the limit of $N_S \gg 1$ in the high-squeezing regime under photon loss.

Let us analyze a measurement based on frequency-resolved photon counting of signal and idler photons for the lossless scenario, which is discussed in detail in Supplementary Note 11. This measurement corresponds to a projection onto the frequency eigenstates $|\boldsymbol{\omega}, \tilde{\boldsymbol{\omega}}\rangle \equiv |\omega_1, \ldots, \omega_n, \tilde{\omega}_1, \ldots \tilde{\omega}_m\rangle \equiv \frac{1}{\sqrt{n!m!}} \otimes_{i=1}^n \otimes_{j=1}^m a^\dagger(\omega_i) b^\dagger(\tilde{\omega}_j)|0\rangle$, where $n, m \in \mathbb{N}$ are the signal and idler photon numbers and $\omega_i, \tilde{\omega}_j \in \mathbb{R}_{>0}$ are the respective frequencies of each photon. The corresponding set of POVM operators are $\{|\boldsymbol{\omega}, \tilde{\boldsymbol{\omega}}\rangle\langle\boldsymbol{\omega}, \tilde{\boldsymbol{\omega}}| | n, m \in \mathbb{N}, \omega_i, \tilde{\omega}_j \in \mathbb{R}_{>0}\}$. We calculate the Fisher information (FI), $\tilde{F}_q$, corresponding to this measurement for a generalization $|\tilde{\psi}_\mu\rangle$ of the probe state $|\psi_\mu\rangle$ given in Eq. (8). This generalized probe state contains phase factors depending on the kinetic properties of the target and a complex squeezing parameter, which were previously omitted in our analysis. We can show that the measurement outcomes do not depend on

these phases. Indeed, both states $|\tilde{\psi}_\mu\rangle$ and $|\psi_\mu\rangle$ give rise to the same probability distribution of measurement outcomes. Thus, the POVM $\{|\boldsymbol{\omega},\tilde{\boldsymbol{\omega}}\rangle\langle\boldsymbol{\omega},\tilde{\boldsymbol{\omega}}|\}$ is actually phase insensitive. Finally, we prove that $\tilde{F}_q = J_q$, so this measurement also saturates the QFI in section "Quantum protocol". Let us remark that this measurement does not depend on the parameter μ, so it can be used for saturating the QFI for any velocity. Also, it could in principle be experimentally feasible by using diffraction gratings that map frequency components to distinct locations where photon counters are placed[53,54]. We note, that the POVM is a separate measurement of the signal and idler beams, which further facilitates the experimental implementation. This also indicates that the idler, and thus the entanglement, solely serves as a state preparation tool. For example, one can check that the idlerless Fock state $\sim(\hat{a}_0^\dagger)^{N_{S0}}(\hat{a}_1^\dagger)^{N_{S1}}|0\rangle$, which has no frequency entanglement and could be approximately heralded with our probe state, beats the SQL and shows the same behaviour under loss as in Eq. (21) for the limit $N_S \gg 1$.

Further perspectives

Lastly, we want to emphasize that the protocol can be easily adapted to different frequency and/or bandwidth estimating protocols. Also, the target's trajectory can be generalized to an accelerating one via a Bogoliubov transformation[55,56], but with an additional complication due to the presence of Casimir radiation. For stationary targets, the protocol can be adapted to estimate the location, which boils down to the estimation of arrival times of the signal beam. The probe state written in the time domain has exactly the same structure as in the frequency domain, where the variances of the double Gaussian change as $\sigma^2/2 \to 2\sigma^2$ and $\epsilon^2/2 \to 2\epsilon^2$. The Schmidt number remains unaltered under this transformation. Thus, the estimation of time arrival of signal photons is analogous to the estimation of mean frequency of the signal photons. Analogously, a measurement that attains the optimal performance is the measurement of photon arrival times.

DISCUSSION

We have proposed a protocol for a quantum Doppler lidar that estimates the radial velocity of a reflecting moving target using a twin beam with frequency entanglement and squeezing as quantum resources. This quantum protocol was benchmarked against a classical one by calculating the QFIs for both strategies. We have identified three different parameter regimes, achieving quantum advantage in two of them. In the high-squeezing regime, where the frequency entanglement becomes less relevant compared to squeezing, the quantum protocol exceeds the standard quantum limit. In the mixed regime, where both quantum resources are comparable, the quantum protocol follows the Heisenberg limit. We have found that frequency-resolved photon counting of signal and idler beam is an optimal measurement in the lossless case. The effect of losses on the performance of the protocol was studied in the high-squeezing regime by modelling the loss channel as a frequency-independent reflectivity beam splitter. A constant factor quantum advantage ≥3 dB in the variance of the estimator is achieved given a path transmissivity ≥50%.

METHODS

Quantum estimation theory

The objective of quantum estimation theory is to find the ultimate precision limit for the estimation of a parameter μ that is encoded in a quantum system. In our scenario, the probe state ρ that is emitted by the lidar acquires information about μ during the reflection off the moving target, which transforms the state as $\rho \to \rho_\mu$. The classical Fisher information (FI) $F(\mu)$ is a measure of the information about the parameter μ that can be extracted by a given measurement corresponding to the positive operator-valued measure (POVM) $\{\Pi_z\}$ with $\int \mathrm{d}z\,\Pi_z = \mathbb{1}$. The FI is given by

$$F(\mu) = \int \mathrm{d}z\,\frac{1}{p_\mu(z)}\left(\partial_\mu p_\mu(z)\right)^2, \tag{22}$$

where $p_\mu(z) = \mathrm{Tr}(\Pi_z\rho_\mu)$ is the probability of having the measurement outcome z given the parameter μ. The Cramér-Rao bound is given by[51]

$$\mathrm{Var}(\bar{\mu}) \geqslant \frac{1}{MF(\mu)}, \tag{23}$$

where $\bar{\mu}$ is an unbiased estimator that maps the measurement data of the M experiment repetitions to an estimate of the parameter μ. The bound can be saturated using the maximum likelihood estimator in the limit of large M[57]. Maximizing the FI over all POVMs $\{\Pi_z\}$ yields the quantum Fisher information $J(\mu) \geqslant F(\mu)$. The Eq. (23) for the QFI is called the quantum Cramér-Rao bound which sets the absolute precision limit for the estimation of μ. In the case of a pure-state manifold, i.e. when $\hat{\rho}_\mu = |\psi_\mu\rangle\langle\psi_\mu|$ for any μ, the QFI is given by[51]

$$J(\mu) = 4\Big(\langle\partial_\mu\psi_\mu|\partial_\mu\psi_\mu\rangle - |\langle\psi_\mu|\partial_\mu\psi_\mu\rangle|^2\Big). \tag{24}$$

To prove a quantum advantage, we calculate the QFIs J_q and J_c of both the quantum and classical strategy. A quantum advantage is achieved, if the ratio is $J_q/J_c > 1$ assuming both strategies illuminate the object with the same energy and an optimal measurement is performed. An observable corresponding to the optimal measurement is given by $\hat{O}_\mu = \mathbb{1}\mu + \hat{L}_\mu/J(\mu)$, where $\hat{L}_\mu$ is the symmetric logarithmic derivative (SLD), which satisfies $\hat{L}_\mu\hat{\rho}_\mu + \hat{\rho}_\mu\hat{L}_\mu = 2\partial_\mu\hat{\rho}_\mu$. As the optimal observable generally depends on the parameter itself, a prior guess about the parameter is required to construct the measurement. The measurement can then be adaptively optimized[52].

Gaussian states

A Gaussian state is fully defined by its first two moments $\mathbf{d}$ and Σ. Their components are defined as

$$d_m = \mathrm{tr}\left[\hat{\rho}\hat{\mathbf{R}}_m\right], \tag{25}$$

and

$$\Sigma_{nm} = \mathrm{tr}\left[\hat{\rho}\{\Delta\hat{\mathbf{R}}_m, \Delta\hat{\mathbf{R}}_n^\dagger\}\right], \tag{26}$$

where $\hat{\mathbf{R}} = (\hat{a}_0, \hat{a}_0^\dagger, \hat{a}_1, \hat{a}_1^\dagger, \dots)^T$ and $\Delta\hat{\mathbf{R}} = \hat{\mathbf{R}} - \hat{\mathbf{d}}$. Gaussian unitaries that transform the state as $\hat{\rho}' = \hat{U}\hat{\rho}\hat{U}^\dagger$ transform the first moments as

$$\mathbf{d}' = \mathbf{G}\mathbf{d} + \mathbf{b}, \tag{27}$$

and

$$\Sigma' = \mathbf{G}\Sigma\mathbf{G}^\dagger, \tag{28}$$

where $\mathbf{G}$ is the corresponding symplectic matrix, see ref. [50] for more information on how $\mathbf{G}$ and $\mathbf{b}$ relate to the Gaussian unitary $\hat{U}$. A formula for the QFI of a Gaussian state is given by

$$J(\mu) = \lim_{\kappa\to 1}\frac{1}{2}\mathrm{vec}[\partial_\mu\Sigma]^\dagger\mathcal{M}_\kappa^{-1}\mathrm{vec}[\partial_\mu\Sigma] + 2\partial_\mu\mathbf{d}^\dagger\Sigma^{-1}\partial_\mu\mathbf{d}, \tag{29}$$

where $\mathcal{M}_\kappa = \kappa\Sigma^\dagger\otimes\Sigma - \mathbf{K}\otimes\mathbf{K}$ with the symplectic form $\mathbf{K} = \mathrm{diag}(1,-1,1,-1,\dots)$. The operation vec[·] turns a matrix into a vector as

$$\mathrm{vec}\left[\begin{pmatrix} a & b \\ c & d \end{pmatrix}\right] = \begin{pmatrix} a \\ b \\ c \\ d \end{pmatrix}. \tag{30}$$

We can also calculate the SLD in this formalism. It is given by

$$\hat{L}_\mu = \Delta\hat{\mathbf{R}}^\dagger \mathcal{A}_\mu \Delta\hat{\mathbf{R}} - \frac{1}{2}\mathrm{tr}[\Sigma\mathcal{A}_\mu] + 2\Delta\hat{\mathbf{R}}^\dagger \Sigma^{-1}\partial_\mu \mathbf{d}, \tag{31}$$

where $\mathrm{vec}[\mathcal{A}_\mu] = \lim_{\kappa\to 1} \mathcal{M}_\kappa^{-1}\mathrm{vec}[\partial_\mu\Sigma]$.

DATA AVAILABILITY

The authors declare that all data supporting the findings of this study are available within the article and its Supplementary Material.

Received: 7 July 2022; Accepted: 30 November 2022;
Published online: 19 December 2022

REFERENCES

1. Pirandola, S., Bardhan, B. R., Gehring, T., Weedbrook, C. & Lloyd, S. Advances in photonic quantum sensing. *Nat. Photonics* **12**, 724–733 (2018).
2. Lloyd, S. Enhanced sensitivity of photodetection via Quantum Illumination. *Science* **321**, 1463–1465 (2008).
3. Tan, S.-H. et al. Quantum illumination with Gaussian states. *Phys. Rev. Lett.* **101**, 253601 (2008).
4. Barzanjeh, S. et al. Microwave quantum illumination. *Phys. Rev. Lett.* **114**, 080503 (2015).
5. Casariego, M., Omar, Y. & Sanz, M. Bi-frequency illumination: a quantum-enhanced protocol. *Adv. Quantum Technol.* **5**, 2100051 (2022).
6. Zhuang, Q., Zhang, Z. & Shapiro, J. H. Quantum illumination for enhanced detection of Rayleigh-fading targets. *Phys. Rev. A* **96**, 020302(R) (2017).
7. Giovannetti, V., Lloyd, S. & Maccone, L. Quantum-enhanced positioning and clock synchronization. *Nature* **412**, 417–419 (2001).
8. Liu, H. et al. Enhancing lidar performance metrics using continuous-wave photon-pair sources. *Optica* **6**, 1349–1355 (2019).
9. Maccone, L. & Ren, C. Quantum radar. *Phys. Rev. Lett.* **124**, 200503 (2020).
10. Zhuang, Q. Quantum ranging with Gaussian entanglement. *Phys. Rev. Lett.* **126**, 240501 (2021).
11. Zhuang, Q. & Shapiro, J. H. Ultimate accuracy limit of quantum pulse-compression ranging. *Phys. Rev. Lett.* **128**, 010501 (2022).
12. Zhuang, Q., Zhang, Z. & Shapiro, J. H. Entanglement-enhanced lidars for simultaneous range and velocity measurements. *Phys. Rev. A* **96**, 040304(R) (2017).
13. Huang, Z., Lupo, C. & Kok, P. Quantum-limited estimation of range and velocity. *PRX Quantum* **2**, 030303 (2021).
14. Huang, Z., Macchiavello, C. & Maccone, L. Usefulness of entanglement-assisted quantum metrology. *Phys. Rev. A* **94**, 012101 (2016).
15. Heras, U. L. et al. Quantum illumination reveals phase-shift inducing cloaking. *Sci. Rep.* **7**, 9333 (2017).
16. Woodworth, T. S., Hermann-Avigliano, C., Chan, K. W. C. & Marino, A. M. Transmission estimation at the Cramér-Rao bound for squeezed states of light in the presence of loss and imperfect detection. *Phys. Rev. A* **102**, 052603 (2022).
17. Woodworth, T. S., Hermann-Avigliano, C., Chan, K. W. C. & Marino, A. M. Transmission Estimation at the Fundamental Quantum Cramér-Rao Bound with Macroscopic Quantum Light. Preprint at https://arxiv.org/abs/2201.08902 (2022).
18. Spedalieri, G., Lupo, C., Braunstein, S. L. & Pirandola, S. Thermal quantum metrology in memoryless and correlated environments. *Quantum Sci. Technol.* **4**, 015008 (2018).
19. Spedalieri, G., Piersimoni, L., Laurino, O., Braunstein, S. L. & Pirandola, S. Detecting and tracking bacteria with quantum light. *Phys. Rev. Res.* **2**, 043260 (2020).
20. Shi, H., Zhang, Z., Pirandola, S. & Zhuang, Q. Entanglement-assisted absorption spectroscopy. *Phys. Rev. Lett.* **125**, 180502 (2020).
21. Pirandola, S. & Lupo, C. Ultimate precision of adaptive noise estimation. *Phys. Rev. Lett.* **118**, 100502 (2017).
22. Lupo, C. & Pirandola, S. Ultimate precision bound of quantum and sub-wavelength imaging. *Phys. Rev. Lett.* **117**, 190802 (2016).
23. Köse, E., Adesso, G. & Braun, D. Quantum-enhanced passive remote sensing. *Phys. Rev. A* **106**, 012601 (2022).
24. Zhuang, Q., Zhang, Z. & Shapiro, J. H. Optimum mixed-state discrimination for noisy entanglement-enhanced sensing. *Phys. Rev. Lett.* **118**, 040801 (2017).
25. Nair, R. & Gu, M. Fundamental limits of quantum illumination. *Optica* **7**, 771–774 (2020).
26. Di Candia, R., Yiğitler, H., Paraoanu, G. S. & Jäntti, R. Two-way covert quantum communication in the microwave regime. *PRX Quantum* **2**, 020316 (2021).
27. Pirandola, S., Laurenza, R., Lupo, C. & Pereira, J. L. Fundamental limits to quantum channel discrimination. *npj Quantum Inf.* **5**, 50 (2019).
28. Zhuang, Q. & Pirandola, S. Ultimate limits for multiple quantum channel discrimination. *Phys. Rev. Lett.* **125**, 080505 (2020).
29. Guha, S. & Erkmen, B. I. Gaussian-state quantum-illumination receivers for target detection. *Phys. Rev. A* **80**, 052310 (2009).
30. Sanz, M., Las Heras, U., García-Ripoll, J. J., Solano, E. & Di Candia, R. Quantum estimation methods for quantum illumination. *Phys. Rev. Lett.* **118**, 070803 (2017).
31. Jonsson, R. & Di Candia, R. Gaussian quantum estimation of the loss parameter in a thermal environment. *J. Phys. A Math. Theor.* **55**, 385301 (2022).
32. Shapiro, J. H. The quantum illumination story. *IEEE Aerosp. Electron. Syst. Mag.* **35**, 8–20 (2020).
33. Jonsson, R., Di Candia, R., Ankel, M., Ström, A. & Johansson, G. A comparison between quantum and classical noise radar sources. In 2020 IEEE Radar Conference (RadarConf20) 1–6 (2020).
34. Shi, H., Zhang, B. & Zhuang, Q. Fulfilling entanglement's benefit via converting correlation to coherence. Preprint at https://arxiv.org/abs/2207.06609 (2022).
35. Arthurs, E. & Kelly, J. L. On the simultaneous measurement of a pair of conjugate observables. *Bell Syst. Tech. J.* **44**, 725–729 (1965).
36. Shapiro, J. H. Quantum pulse compression laser radar. *Proc. SPIE Int. Soc. Opt. Eng.* **6603**, 660306 (2007).
37. Van Trees, H. L. *Detection, Estimation, and Modulation theory, Part III: Radar-Sonar Signal Processing and Gaussian Signals in Noise* (Wiley, 2001).
38. Mosley, P. J., Christ, A., Eckstein, A. & Silberhorn, C. Direct measurement of the spatial-spectral structure of waveguided parametric down-conversion. *Phys. Rev. Lett.* **103**, 233901 (2009).
39. Christ, A. et al. Spatial modes in waveguided parametric down-conversion. *Phys. Rev. A* **80**, 033829 (2009).
40. Christ, A., Laiho, K., Eckstein, A., Cassemiro, K. N. & Silberhorn, C. Probing multimode squeezing with correlation functions. *N. J. Phys.* **13**, 033027 (2011).
41. Horn, R. et al. Monolithic source of photon pairs. *Phys. Rev. Lett.* **108**, 153605 (2012).
42. Francesconi, S. et al. Engineering two-photon wavefunction and exchange statistics in a semiconductor chip. *Optica* **7**, 316–322 (2020).
43. Eckstein, A., Christ, A., Mosley, P. J. & Silberhorn, C. Highly efficient single-pass source of pulsed single-mode twin beams of light. *Phys. Rev. Lett.* **106**, 013603 (2011).
44. Merkouche, S., Thiel, V. & Smith, B. J. Spectrally resolved four-photon interference of time-frequency-entangled photons. *Phys. Rev. A* **105**, 023708 (2022).
45. Fedorov, M., Mikhailova, Y. M. & Volkov, P. Gaussian modelling and Schmidt modes of SPDC biphoton states. *J. Phys. B* **42**, 175503 (2009).
46. Xie, Z. et al. Harnessing high-dimensional hyperentanglement through a biphoton frequency comb. *Nat. Photonics* **9**, 536–542 (2015).
47. Blow, K. J., Loudon, R., Phoenix, S. J. D. & Shepherd, T. J. Continuum fields in quantum optics. *Phys. Rev. A* **42**, 4102 (1990).
48. Barnett, S. & Radmore, P. M. *Methods in Theoretical Quantum Optics* (Oxford University Press, 2002)
49. Davis, A. O., Saulnier, P. M., Karpiński, M. & Smith, B. J. Pulsed single-photon spectrometer by frequency-to-time mapping using chirped fiber bragg gratings. *Opt. Express* **25**, 12804 (2017).
50. Šafránek, D. Estimation of Gaussian quantum states. *J. Phys. A Math. Theor.* **52**, 035304 (2019).
51. Paris, M. G. Quantum estimation for quantum technology. *Int. J. Quantum Inf.* **7**, 125–137 (2009).
52. Liu, J., Yuan, H., Lu, X.-M. & Wang, X. Quantum Fisher information matrix and multiparameter estimation. *J. Phys. A Math. Theor.* **53**, 023001 (2019).
53. Gianani, I., Sbroscia, M. & Barbieri, M. Measuring the time-frequency properties of photon pairs: a short review. *AVS Quantum Sci.* **2**, 011701 (2020).
54. Davis, A. O., Thiel, V. & Smith, B. J. Measuring the quantum state of a photon pair entangled in frequency and time. *Optica* **7**, 1317 (2020).
55. Gianfelici, G. & Mancini, S. Quantum channels from reflections on moving mirrors. *Sci. Rep.* **7**, 115747 (2017).
56. Good, M. R. R., Anderson, P. R. & Evans, C. R. Time dependence of particle creation from accelerating mirrors. *Phys. Rev. D.* **88**, 025023 (2013).
57. Fisher, R. A. Theory of statistical estimation. *Math. Proc. Camb. Philos. Soc.* **22**, 700–725 (1925).

ACKNOWLEDGEMENTS

We thank Robert Jonsson, Göran Johansson and Benjamin Huard for insightful discussions. We acknowledge financial support from Basque Government QUANTEK project from ELKARTEK program (KK-2021/00070) and the Basque Government project IT1470-22, Spanish Ramón y Cajal Grant RYC-2020-030503-I and the project grant PID2021-125823NA-I00 funded by MCIN/AEI/10.13039/501100011033 and by "ERDF A way of making Europe" and "ERDF Invest in your Future", as well as from QMiCS (820505) and OpenSuperQ (820363) projects of the EU Flagship on Quantum Technologies, and the EU FET-Open projects Quromorphic (828826) and EPIQUS

(899368). M.R. acknowledges support from UPV/EHU PhD Grant PIF21/289. M.W. acknowledges support from the National Science Foundation under Grant CCF-1956211. R.D.C. acknowledges support from the Marie Skłodowska Curie fellowship number 891517 (MSC-IF Green- MIQUEC), the Alexander von Humboldt Foundation, the Knut and Alice Wallenberg Foundation through the Wallenberg Centre for Quantum Technology (WACQT), and the Academy of Finland, grants nos. 353832, 349199.

AUTHOR CONTRIBUTIONS

M.R. developed the theoretical formalism and performed the analytic calculations. M.S. suggested the seminal idea and supervised the project throughout all stages. M.R., M.S., R.D.C. and M.W. contributed to the interpretation and improvement of the results. M.R. took the lead in writing the manuscript and all authors provided critical feedback.

COMPETING INTERESTS

The authors declare no competing interests.

ADDITIONAL INFORMATION

Supplementary information The online version contains supplementary material available at https://doi.org/10.1038/s41534-022-00662-9.

Correspondence and requests for materials should be addressed to Maximilian Reichert or Mikel Sanz.